Electronic Supplementary Material (ESI) for Energy & Environmental Science.

Supporting Information

Hierarchical CoP/Ni_5P_4/CoP microsheet arrays as a robust pH-universal electrocatalyst for efficient hydrogen generation

Ishwar Kumar Mishra, Haiqing Zhou, Jingying Sun, Keshab Dahal, Shuo Chen, and Zhifeng Ren**

*Correspondence and requests for materials should be addressed to S. C. schen34@ uh.edu and Z. F. R. zren@uh.edu.

1. Experimental details

Chemicals. Cobalt (II) nitrate hexahydrate ($Co(NO_3)_2 \cdot 6H_2O$, 98%, Sigma-Aldrich), N,N-Dimethylformamide [$(CH_3)_2NC(O)H$, anhydrous, 99.8%, Sigma-Aldrich], red phosphorous powder (P, ≥ 97%, Sigma-Aldrich), sulfuric acid (H_2SO_4, ACS 95.0-98.0%, Alfa Aesar) potassium hydroxide (KOH, 50% w/v, Alfa Aesar), and Ni foam (thickness: 1.6 mm), graphite foil (Alfa Aesar), and Pt wire (CH Instruments). Deionized water (resistivity: 18.2 MΩ·cm) was used for the preparation of all aqueous solutions. All the chemicals were of analytical grade and utilized without further purification.

Synthesis of Ni_5P_4-Ni_2P nanosheet arrays on Ni foam. The as-obtained commercial Ni foam was usually cut into 1 cm^2 regular pieces. For growing Ni_5P_4-Ni_2P/Ni nanosheet arrays support, one piece of 1 cm^2 Ni foam was placed in the tube furnace, which was heated to 500 ^oC quickly and kepted at this temperature for around 1 hour for thermal phosphorization in argon atmosphere. The red phosphorus powder was used as the phosphorus source putting at the upstream. After material growth, we shut down the power of the tube furnace and waited it to be naturally cooled down under argon protection.

Synthesis of CoP/Ni_5P_4/CoP microsheet arrays electrocatalyst. For the synthesis of CoP/Ni_5P_4/CoP microsheet arrays electrocatalyst, the cobalt precursor ink was prepared by dissolving cobalt nitrate hexahydrate [$Co(NO_3)_2.6H_2O$] in N,N dimethylformamide (DMF), then the nickel phosphide nanosheet arrays on Ni foam (Ni_5P_4-Ni_2P/Ni) was soaked in the Co-ink and dried at ambient condition. The dried sample was then thermally phosphorized at 500 ^oC in a tube furnace with the red phosphorus powder placed at upstream, which resulted in the formation of hierarchical CoP/Ni_5P_4/CoP microsheet arrays.

Nitrogen adsorption measurements. The samples were firstly dried in vacumm at 373 K for 12 h before measurement. Nitrogen adsorption-desorption isotherms were tested at 77 K by a Quantachrome Autosorb-iQ BET surface analyzer. The specific surface area was evaluated from the BET method, and the distribution of pore sizes was analyzed by the BJH method.

Electrochemical measurements. We carried out the electrochemical tests at room temperature via a three-electrode configuration using Gamry Instruments, Reference 600. An 82 mL 0.5 M H_2SO_4 was added into the cell for HER as acidic electrolyte, and 100 ml of 1.0 M KOH was used for HER as alkaline electrolyte. Saturated calomel electrode (SCE) and Hg/HgO electrode were used as the reference electrodes in acidic and alkaline electrolytes, respectively. Graphite foil (Alfa Aesar) was used as the counter electrode and the self-supported catalysts were directly connected with the working electrode. To study the catalytic performance, we collected the polarization curves under a sweep rate of 2 mV s^{-1} with the potentials ranging from 0.050 V to - 0.150 V *vs* RHE. High-purity anhydrous N_2 gas (Matheson, 99.9999%) was used to purge the system for 30 minutes before any measurements. In acidic electrolyte, the measured potentials *vs* SCE were converted to RHE by the Nernst equation ($E_{\mathrm{RHE}} = E_{\mathrm{SCE}} + 0.0591 \mathrm{pH} + 0.245$). We continuously cycled the catalyst for over 1000 cycles at a scan rate of 50 mV s^{-1}, so as to check its electrochemical stability. Chronopotentiometry test was conducted at cathodic current densities of -30 mA cm^{-2} and -1 A cm^{-2} for more than 25 hours. For the high current densities, durability test at -500 mA cm^{-2} and -1 A cm^{-2}, Pt wire was used as counter electrode since graphite was not stable over a long time. In all other measurements, graphite foil was used as the counter electrode. The electrochemical impedance spectroscopy (EIS) spectrum was tested at -0.150 V vs RHE with the frequency changing from 0.1 Hz to 0.1 MHz with a 10 mV AC dither. All the potentials used here are referred to RHE unless otherwise mentioned. Electrochemical tests were performed at room temperature and the curves were reported with *iR* compensation. In alkaline electrolyte, the measured potentials *vs* Hg/HgO were converted to RHE by the Nernst equation ($E_{RHE} = E_{Hg/HgO} + 0.0591$ pH + 0.098).

Calculation of turnover frequency (TOF). Due to the bulk feature of our catalyst CoP/Ni_5P_4/CoP, we selected an electrochemical method[2,3] to obtain the active site density at the surface. Here we suppose that nearly all the surface active sites are accessible to the electrolyte, then it is possible to evaluate the TOF values by the equation as follows:

$$TOF = \frac{1}{2}\frac{I}{nF} \qquad (1)$$

Here these physical variables F, n, and *I* represent the Faraday constant (~ 96485 C/mol), active site density (mol), and the current (A) during hydrogen evolution in 0.5 M H_2SO_4, respectively. The factor 1/2 is because water electrolysis requires two electrons to evolve one hydrogen molecule from two protons.

The electrochemical measurements were performed to collect the CV curves in 1M PBS electrolyte (pH = 7). Actually, it is very difficult to assign the observed peaks to a given redox couple, so the surface active sites are nearly in linear relationship with the integrated voltammetric charges (cathodic and anodic) over the CV curves. Assuming a one-electron process for both reduction and oxidation, we can evaluate the upper limit of the active site number (n) according to the follow formula:

$$n = \frac{Q}{2F} \qquad (2)$$

Here F and Q correspond to the Faraday constant and the whole charge of CV curve, respectively. In this case, we can deduce the number of active sites for this sandwich-like catalyst CoP/Ni_5P_4/CoP is close to 7.43×10^{-7} mol/cm^2. Thus, we can calculate the TOF values to be around 0.453 and 1.220 s^{-1} for the CoP/Ni_5P_4/CoP catalyst at overpotentials of 75 and 100 mV, respectively.

Faradaic efficiency determination. A technique based on gas chromatography (GC)[1] was used to quantify the gas products and then the Faradaic efficiency under a constant current density of -50 mA cm^{-2}. For every 10 min, we used a glass syringe to carefully take 0.3 mL gas product from the sealed cell and injected it into the GC instrument (GOW-MAC 350 TCD) (Hamilton Gastight 1002). Based on this technique, we find that H_2 gas is the only product in experiment, which is nearly the same amount as that by theoretical calculations, supposing that each electron was utilized for H_2 generation.

2. Morphology, material structure, and composition

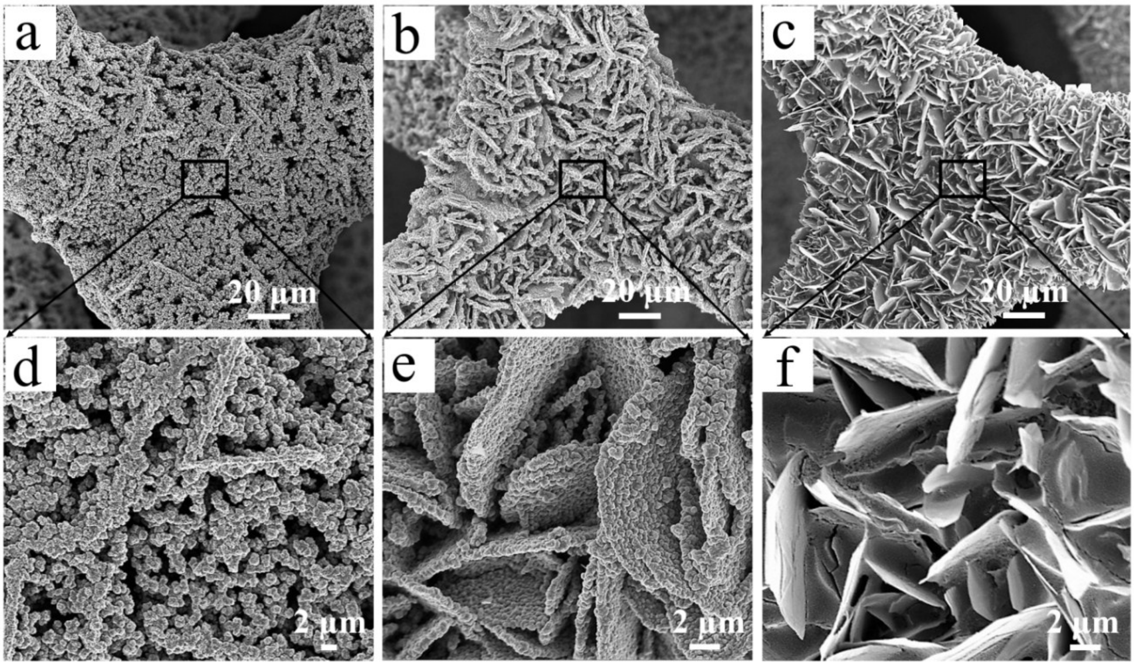

Figure S1. SEM images of CoP/Ni_5P_4/CoP samples prepared with Co-ink concentrations of (a, d) 0.4 g/ml, (b, e) 0.25 g/ml, and (c, f) 0.1 g/ml.

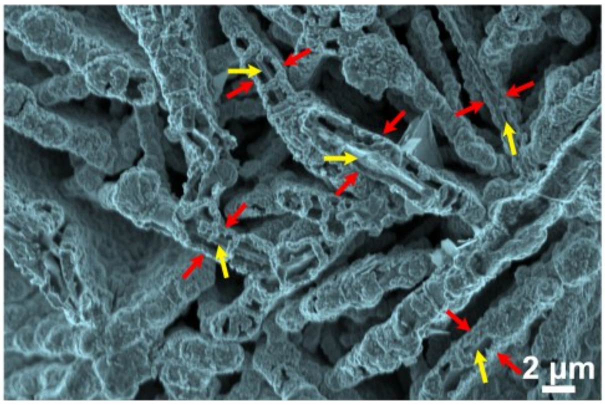

Figure S2. A typical SEM image showing the sandwich-like structures of CoP/Ni_5P_4/CoP when CoP particles are in-situ grown on the surfaces of nickel phosphide nanosheet arrays. The red and yellow arrows indicate the CoP and Ni_5P_4 nanosheet parts, respectively.

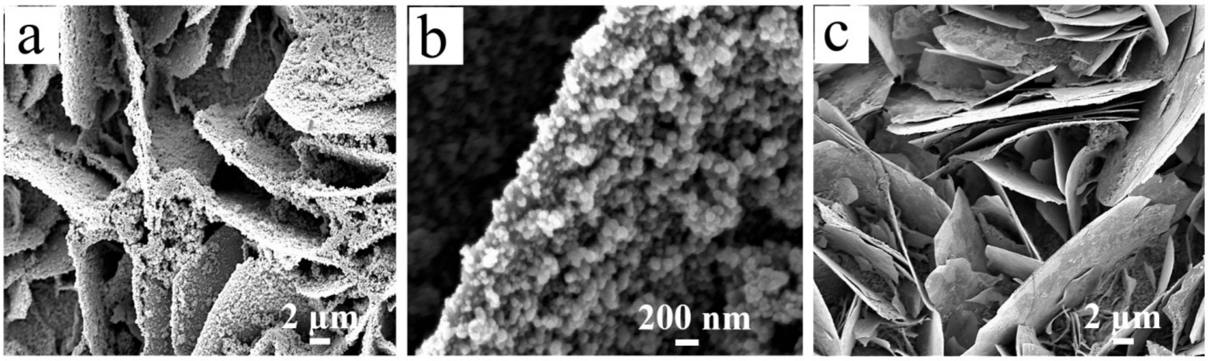

Figure S3. SEM images of samples prepared with annealing in the absence of phosphorus at the third step of synthesis. (a, b) Before electrochemical test. (c) After electrochemical test in 0.5 M H_2SO_4.

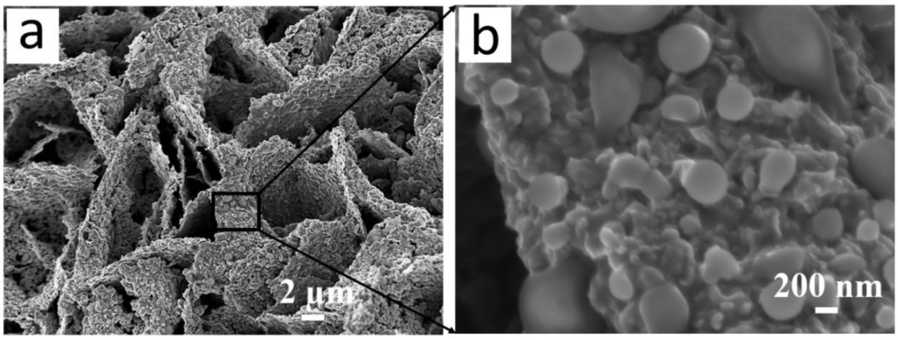

Figure S4. (a,b) SEM images of sample prepared at 600 ^{o}C at the third step of synthesis. High resolution SEM image on the right side.

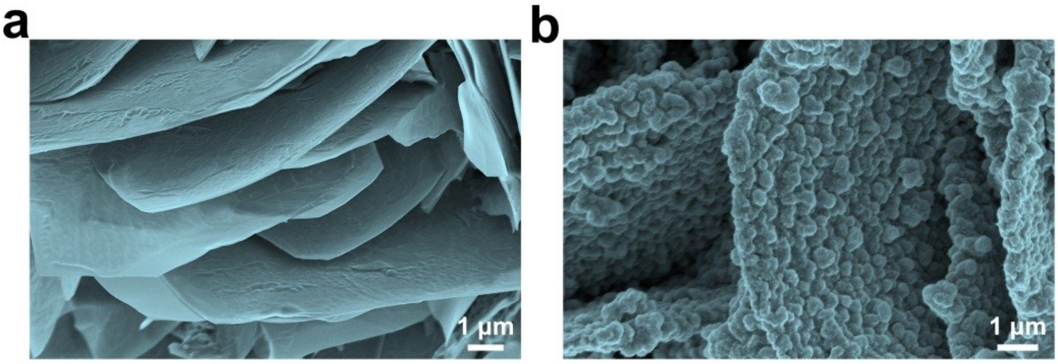

Figure S5. Comparison of the SEM morphologies between original Ni_5P_4-Ni_2P/Ni and CoP/Ni_5P_4/CoP catalysts.

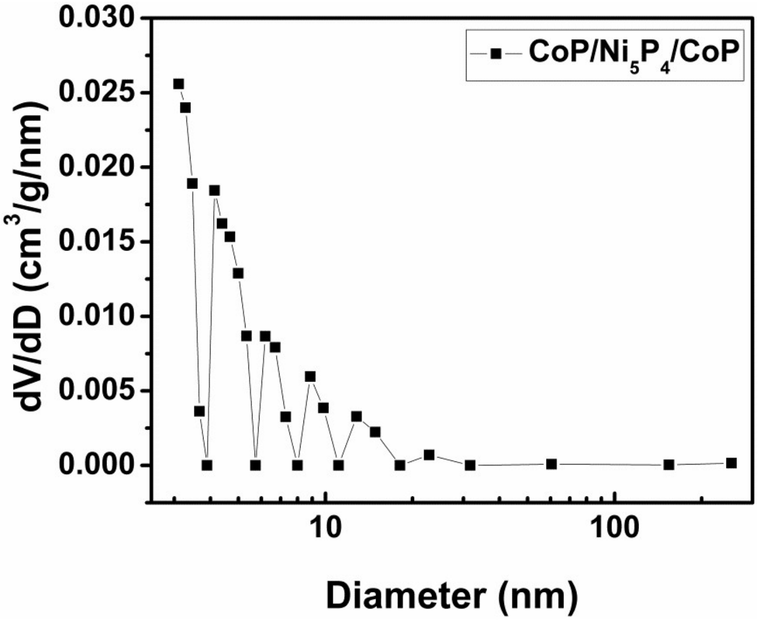

Figure S6. The distribution of mesopore sizes of the sandwich-like CoP/Ni_5P_4/CoP electrocatalysts measured by the BJH method.

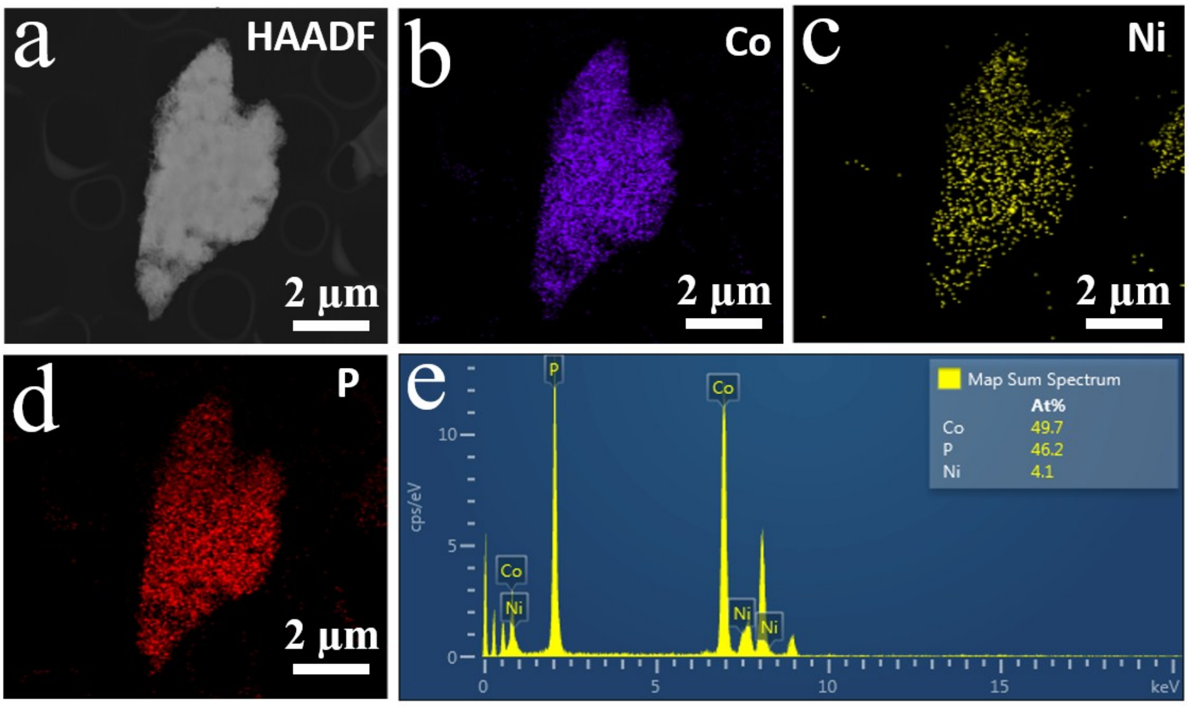

Figure S7. EDS elemental mapping images of as-prepared CoP/Ni_5P_4/CoP. (a) HAADF. (b) Co. (c) Ni. (d) P. (e) EDS spectra of CoP/Ni_5P_4/CoP.

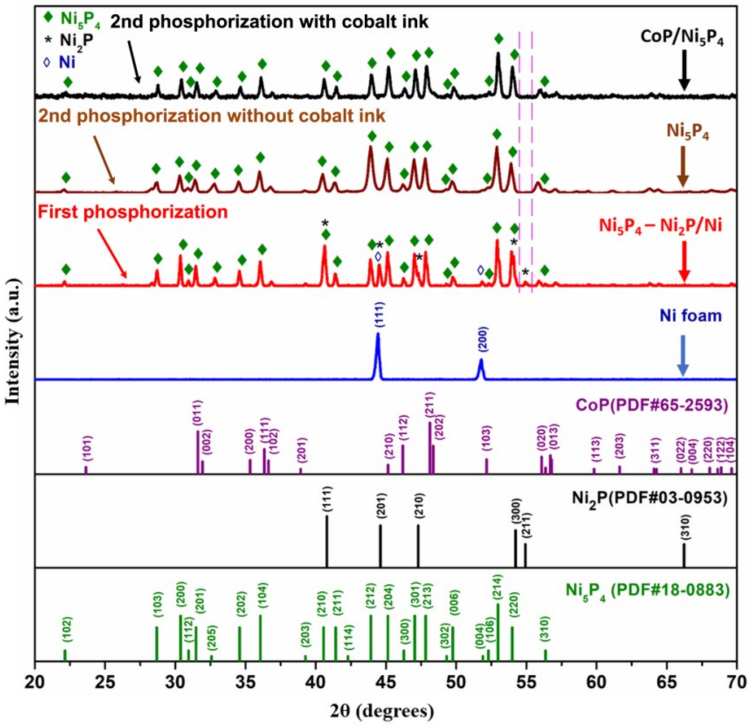

Figure S8. Comparison of the XRD patterns of the nickel phosphide nanosheets after the 2nd phosphorization or 1st phosphorization at 500 ^{o}C without cobalt ink, and $CoP/Ni_5P_4/CoP$ using cobalt ink.

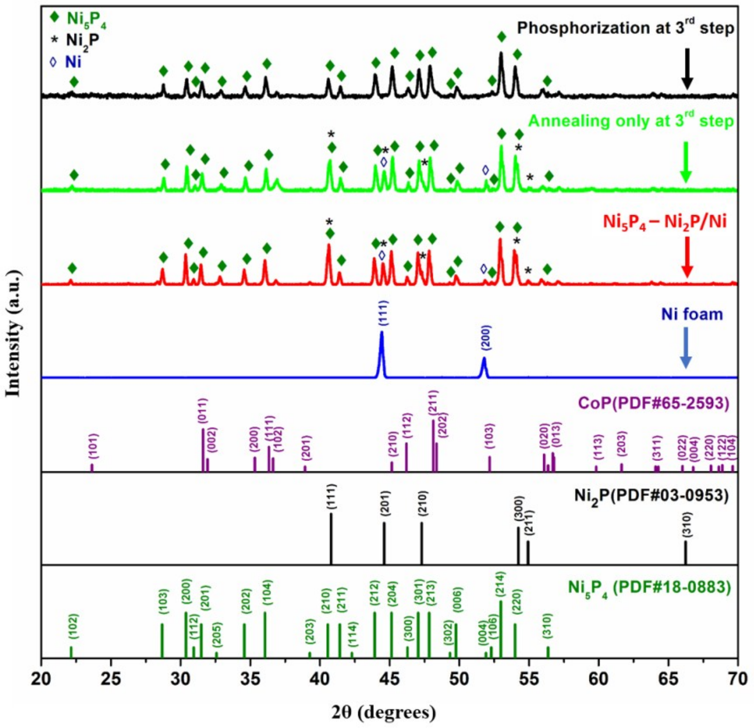

Figure S9. Comparison of XRD patterns between the samples prepared with and without phosphorus source at the third synthetic step.

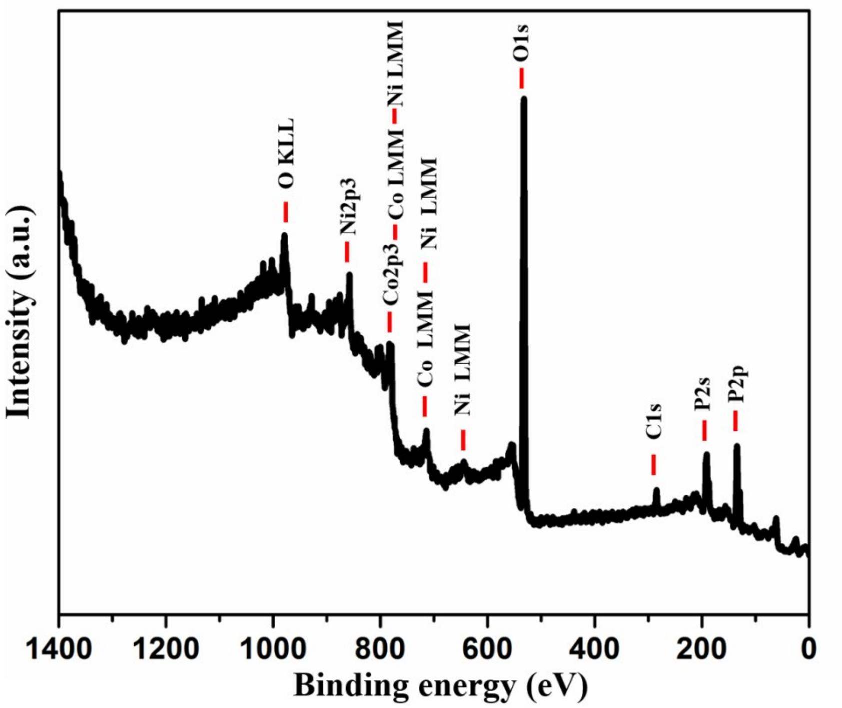

Figure S10. XPS survey spectra of as-prepared CoP/Ni_5P_4/CoP electrode.

Table S1. Detailed analysis of XPS binding energies of different elements for CoP/Ni_5P_4/CoP catalyst.

XPS Peak for	Binding Energy (eV)	
	Before HER test	After HER test
Co $2p^{3/2}$ in CoP	779.6	779.5
Co $2p^{3/2}$ in $CoPO_x$	782.9	782.2
Satellite peak	787.5	786.1
Co $2p^{1/2}$ in CoP	794.8	794.7
Co $2p^{1/2}$ in $CoPO_x$	798.1	797.4
Satellite peak	803.7	803.3
Ni $2p^{3/2}$	857.6	857.0
Satellite peak of Ni $2p^{3/2}$	863.6	862.6
Ni $2p^{1/2}$	875.1	874.5
Satellite peak of Ni $2p^{1/2}$	880.9	879.9
P $2p^{3/2}$	129.6	129.8
P $2p^{1/2}$	130.5	130.6
PO_x $2p^{3/2}$	134.3	133.3
PO_x $2p^{1/2}$	135.1	134.2

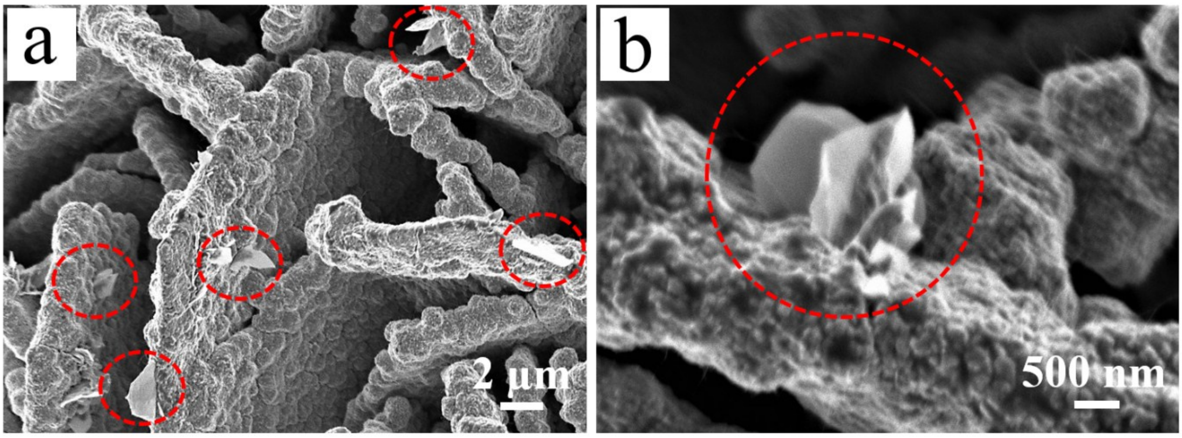

Figure S11. SEM images of as-prepared CoP/Ni_5P_4/CoP sample. (a,b) Showing protruded parts of nickel phosphide nanosheets after phosphorization at the third synthetic step. High resolution SEM image on the right side.

3. Electrochemical performance

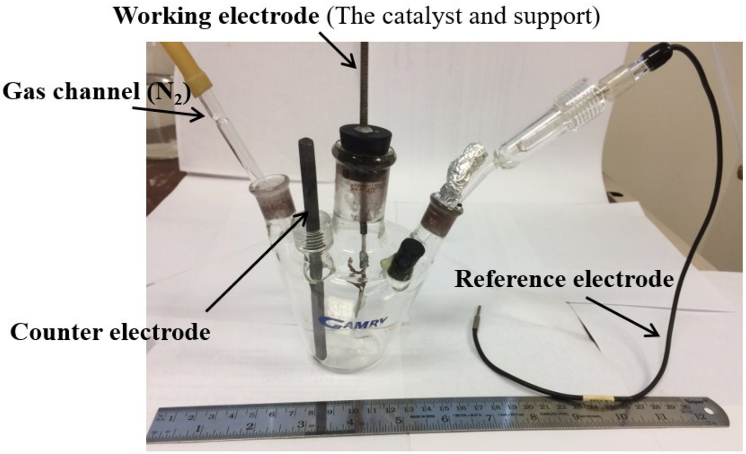

Figure S12. A photograph of the three-electrode setup for electrochemical tests. Normally a graphite rod or graphite paper was used as the counter electrode.

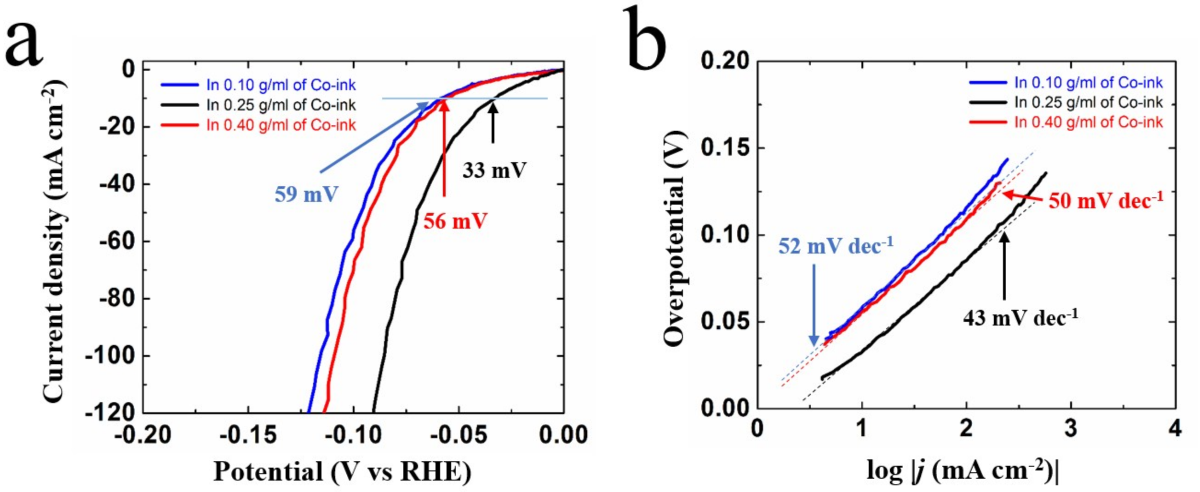

Figure S13. Electrochemical performance of CoP/Ni_5P_4/CoP samples prepared with different concentrations of Co-ink. (a) Polarization curves. (b) Corresponding Tafel plots of the samples in (a).

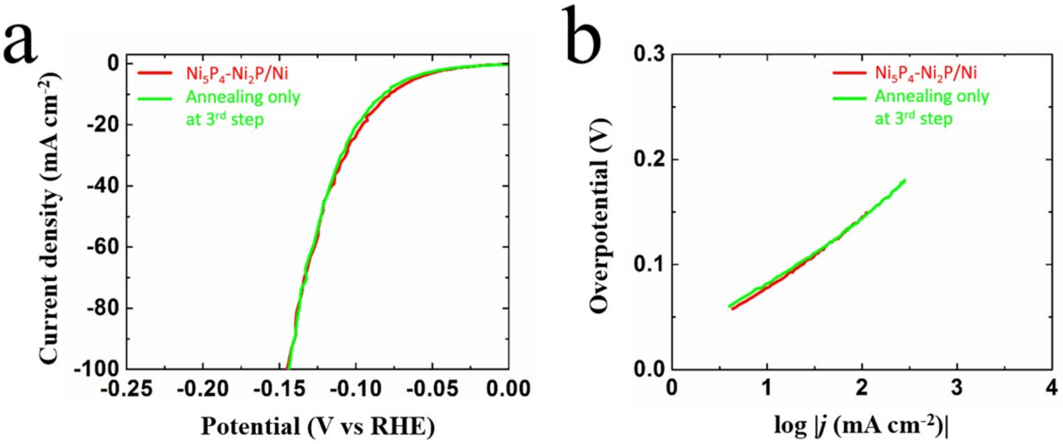

Figure S14. Electrochemical performance comparison between samples prepared with annealing in the absence of phosphorus at the third step of synthesis and Ni_5P_4-NiP_2/Ni support in 0.5 M H_2SO_4. (a) Polarization curves. (b) Corresponding Tafel plots of the samples in (a).

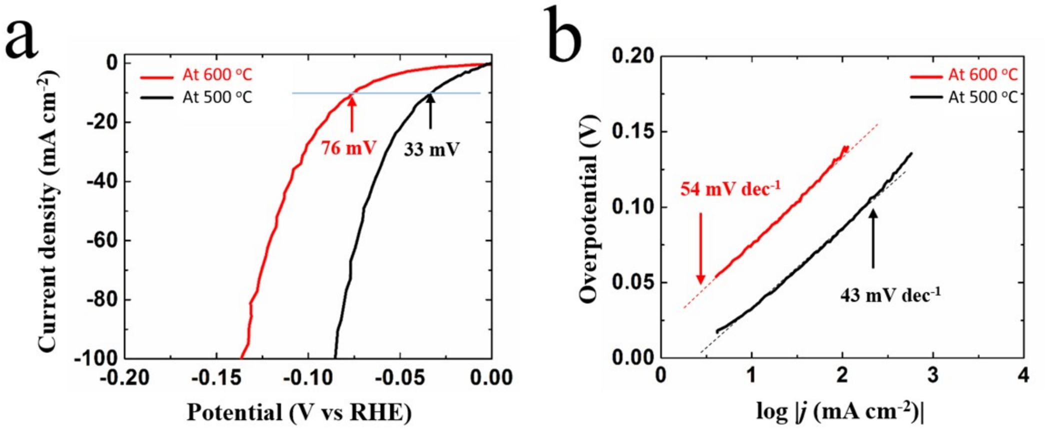

Figure S15. Electrochemical performance comparison between samples prepared at 500 °C and 600 °C at the third step of synthesis. (a) Polarization curves. (b) Corresponding Tafel plots of the samples in (a).

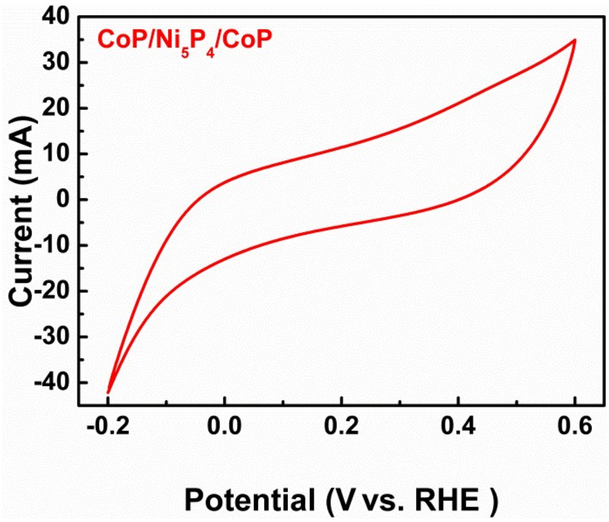

Figure S16. CV curves recorded on the CoP/Ni_5P_4/CoP electrode in the potential ranges between -0.2 V vs RHE and 0.6 V vs RHE in 1 M PBS. The scan rate was 50 mV s^{-1}.

4. Catalytic activity comparison

Table S2. The catalytic performance of our as-obtained HER catalyst in comparison with other available non-precious catalysts in the literatures. Here, η_{10}, η_{100}, and η_{1000} are denoted as the overpotentials at current density of 10, 100, and 1000 mA cm^{-2}, respectively, and j_0 is the exchange current density. Electrolyte: 0.5 M H_2SO_4.

Catalysts	j_0	η_{10}	η_{100}	η_{1000}	**Tafel slope**	**Source**
CoP/Ni_5P_4/CoP	1.708 mA cm^{-2}	33 mV	85 mV	142 mV	43 mV dec^{-1}	This work
$Fe_{0.5}Co_{0.5}P$	584.4 μA cm^{-2*}	37 mV	98 mV	NA	30 mV dec^{-1}	4
CoPS NPls	984 μA cm^{-2}	48 mV	NA	NA	56 mV dec^{-1}	5
Ni_5P_4-NiP_2 NS	636.6 μA cm^{-2}	61 mV	121 mV	NA	51 mV dec^{-1}	6
CoNiP	537 μA cm^{-2}	60 mV	NA	NA	39 mV dec^{-1}	7
CoP nanowires	288 μA cm^{-2}	67 mV	204 mV	NA	51 mV dec^{-1}	8
CoP nanosheets	233 μA cm^{-2*}	49 mV	94 mV	NA	30 mV dec^{-1}	9
np-$(Co_{0.52}Fe_{0.48})_2P$	0.5 mA cm^{-2}	64 mV	NA	NA	45 mV dec^{-1}	10
CoP/Ti foil	0.14 mA cm^{-2}	75 mV*	NA	NA	50 mV dec^{-1}	11
CoP/CNT	0.13 mA cm^{-2}	122 mV	NA	NA	54 mV dec^{-1}	12
Co_2P nanorods	0.129 mA cm^{-2*}	134 mV	NA	NA	71 mV dec^{-1}	13
Ce-doped CoP	1.0 mA cm^{-2*}	54 mV	120 mV	NA	54 mV dec^{-1}	14
Ni_2P nanoparticles	33 μA cm^{-2}	105 mV	180 mV	NA	46 mV dec^{-1}	15
$Ni_{12}P_5$/Ti foil	NA	107 mV	NA	NA	63 mV dec^{-1}	16
FeP nanorods	0.5 mA cm^{-2}	58 mV	~ 200 mV	NA	45 mV dec^{-1}	17
FeP nanowire arrays	0.42 mA cm^{-2}	55 mV	127 mV	NA	38 mV dec^{-1}	18
Cu_3P nanowires	0.18 mA cm^{-2}	143 mV	276 mV	NA	67 mV dec^{-1}	19
CoS|P/CNT	1.140 mA cm^{-2}	48 mV	109 mV	NA	55 mV dec^{-1}	20
CoMoP	1.21 mA cm^{-2}	41 mV	NA	NA	49.73 mV dec^{-1}	21
Mo-W-P/CC	288 μA cm^{-2}	100 mV	138 mV	NA	52 mV dec^{-1}	22
WP_2 nanowires	130 μA cm^{-2}	109 mV	160 mV	NA	56 mV dec^{-1}	23
MoP particles	34 μA cm^{-2}	140 mV	350 mV	NA	54 mV dec^{-1}	24
MoP nanoparticles	86 μA cm^{-2}	125 mV	200 mV	NA	54 mV dec^{-1}	25
MoP|S	0.57 mA cm^{-2}	64 mV	120 mV	NA	50 mV dec^{-1}	26
$MoS_{2(1-x)}Se_{2x}/NiSe_2$	299 μA cm^{-2}	69 mV	112 mV	NA	42 mV dec^{-1}	1
$WS_{2(1-x)}Se_{2x}/NiSe_2$	215 μA cm^{-2}	88 mV	141 mV	NA	47 mV dec^{-1}	27
Metallic FeNiS NS	20 μA cm^{-2}	105 mV	180 mV	NA	40 mV dec^{-1}	28
$CoSe_2$/carbon fiber	6 μA cm^{-2}	139 mV	184 mV	NA	42 mV dec^{-1}	29
Porous $NiSe_2$	612.0 μA cm^{-2}	57 mV	103 mV	NA	43.0 mV dec^{-1}	30

NA: Not applicable since not reported. The symbol "*" means that the value is extracted on the basis of the Tafel slope and overpotential at 10 mA cm^{-2}.

Table S3. Comparison of the catalytic parameters among our catalyst and other robust non-precious catalysts reported thus far. $C_{dl,}$ ECSA, TOF_{75}, and TOF_{100} represent double-layer capacitance, electrochemical surface area, and turnover frequecies at overpotentials of 75 and 100 mV, respectively. Electrolyte: 0.5 M H_2SO_4.

Catalysts	C_{dl} (mFcm^{-2})	**ECSA (cm^2)**	**Roughness factor (RF)**	**Site density**	TOF_{75} (s^{-1})	TOF_{100} (s^{-1})	**Source**
CoP/Ni_5P_4/CoP	144.5	3211	3211	7.43×10^{-7} mol/cm^2	0.453	1.220	This work
$Fe_{0.5}Co_{0.5}P$	32	711.1	711.1	NA	NA	NA	4
CoPS NPls	99.6	2213.3	2213.3	NA	NA	NA	5
Ni_5P_4-NiP_2	66.6	1480	1480	$4.78\times10^{-6*}$ mol/cm^2	0.016*	0.039*	6
CoP nanosheets	172.5	3833	3833	1.29×10^{-6} mol/cm^2	0.187	0.516	9

$Co_{1.04}Fe_{0.96}P$	42.0*	928*	928*	3.11×10^{-6} mol/cm^2	0.027	0.1	10
CoP/Ti foil	NA	NA	NA	2.74×10^{-6} mol/cm^2	NA	0.046	11
Co_2P nanorods	NA	NA	NA	$9.0\times10^{-8*}$ mol/cm^2	0.09*	0.213*	13
Ce-doped CoP	42.2	937.8*	937.8*	NA	0.154*	0.36	14
Ni_2P nanoparticles	NA	NA	NA	1.36×10^{-6} mol/cm^2	NA	0.015	15
FeP nanorods	60	1333	1333	NA	NA	NA	17
Cu_3P nanowires	77.8	1728.9	1728.9	NA	NA	NA	19
Mo-W-P nanosheet	70.8	1573.3	1573.3	4.4×10^{-6} mol/cm^2	0.008*	0.02*	22
MoP nanoparticles	14.4	360	360	1.01×10^{-6} mol/cm^2	0.006	0.024	26
MoP|S	12.2	305	305	8.56×10^{-7} mol/cm^2	0.04	0.13	26
$MoS_{2(1-x)}Se_{2x}$/ $NiSe_2$	319	5316	5316	9.71×10^{-6} mol/cm^2	NA	0.03	1

NA: Not applicable since not reported. The symbol "*" means that the value is extracted on the basis of the data provided in the references. The C_{dl} and ECSA values were calculated by the method proposed in our previous paper,[1] supposing that the flat electrode has a specific capacitance of 45 μF cm^{-2} in 0.5 M H_2SO_4. Also, the active sites of metal phosphides were calculated according to this reference[31] once the capacitance was provided in the relevant references.

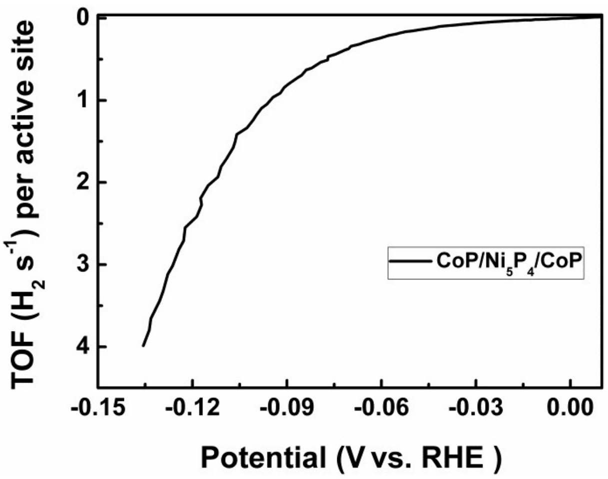

Figure S17. TOF values of the CoP/Ni_5P_4/CoP electrode varied with the HER potentials.

5. EIS fiting model

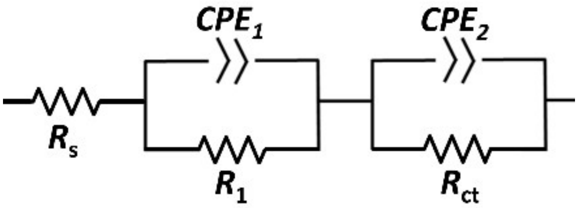

Figure S18. Simplified Randles model used to fit the EIS data.

6. Capacitance measurements

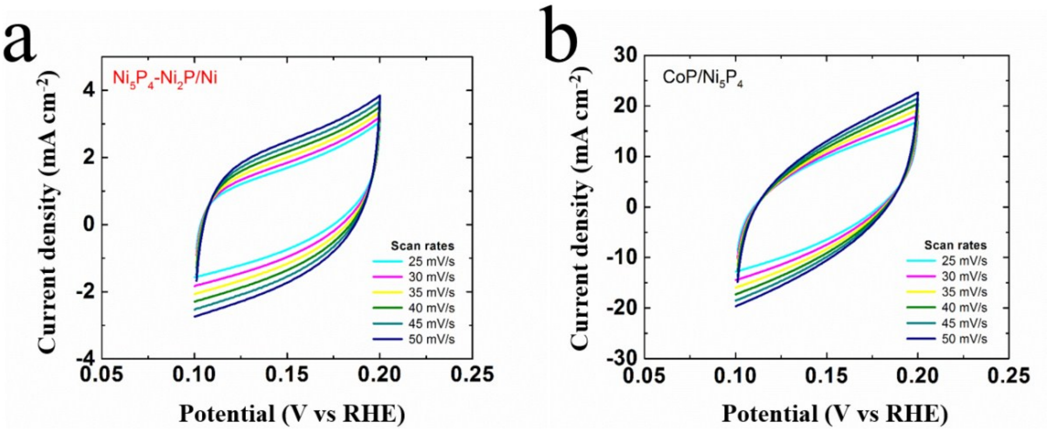

Figure S19. Electrochemical measurements of the double-layer capacitance of different electrodes. (**a**) Ni_5P_4-Ni_2P/Ni. (**b**) CoP/Ni_5P_4/CoP.

Table S4. Summary of the catalytic activities from the Ni_5P_4-Ni_2P/Ni and CoP/Ni_5P_4/CoP electrodes. $j_{0,\text{normalized}}$ is the normalized current density by relative surface area. The electrochemical surface area (ECSA) was calculated by dividing double-layer capacitance (C_{dl}) by the specific capacitance (C_s = 45 μF cm^{-2}) of flat electrodes in 0.5 M H_2SO_4.[22]

Catalysts	η_{10}	Tafel slope	C_{dl}	ECSA	$j_{0,\text{ geometric}}$	Relative surface area	$j_{0,\text{ normalized}}$
Ni_5P_4-Ni_2P/Ni	79 mV	55 mV dec^{-1}	35.4 mF cm^{-2}	786 cm^2_{ECSA}	366.1 μA cm^{-2}	1	366.1 μA cm^{-2}
CoP/Ni_5P_4/CoP	33 mV	43 mV dec^{-1}	144.5 $mFcm^{-2}$	3211 cm^2_{ECSA}	1708.2 μA cm^{-2}	4.1	625.6 μA cm^{-2}

7. Structure, phase, and surface chemical composition of the CoP/Ni_5P_4/CoP sample before and after electrochemical test

H_2SO_4.

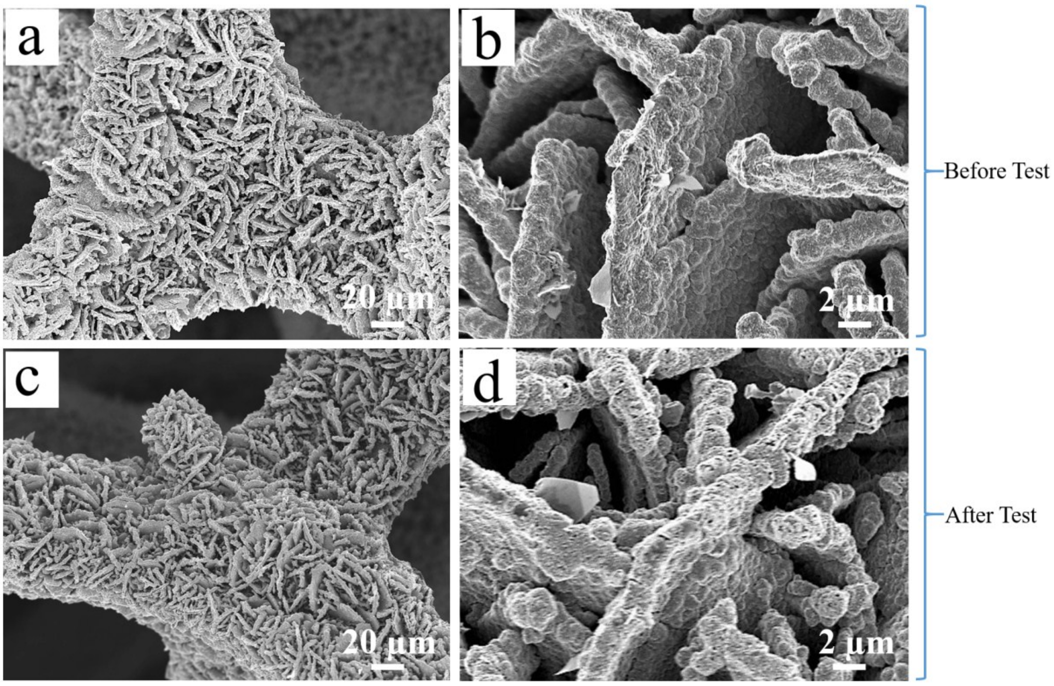

Figure S20. SEM images of as-prepared CoP/Ni_5P_4/CoP sample. (a,b) Before electrochemical test. (c,d) After electrochemical test in 0.5 M H_2SO_4. High resolution SEM images on the right sides.

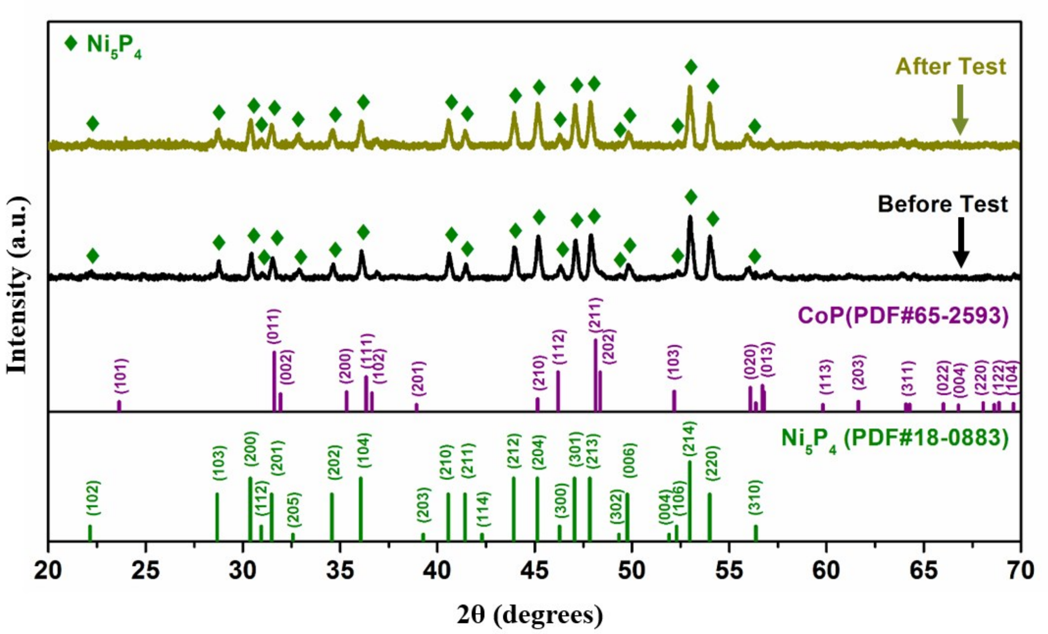

Figure S21. XRD patterns of the CoP/Ni_5P_4/CoP electrode before and after electrochemical test in 0.5 M H_2SO_4.

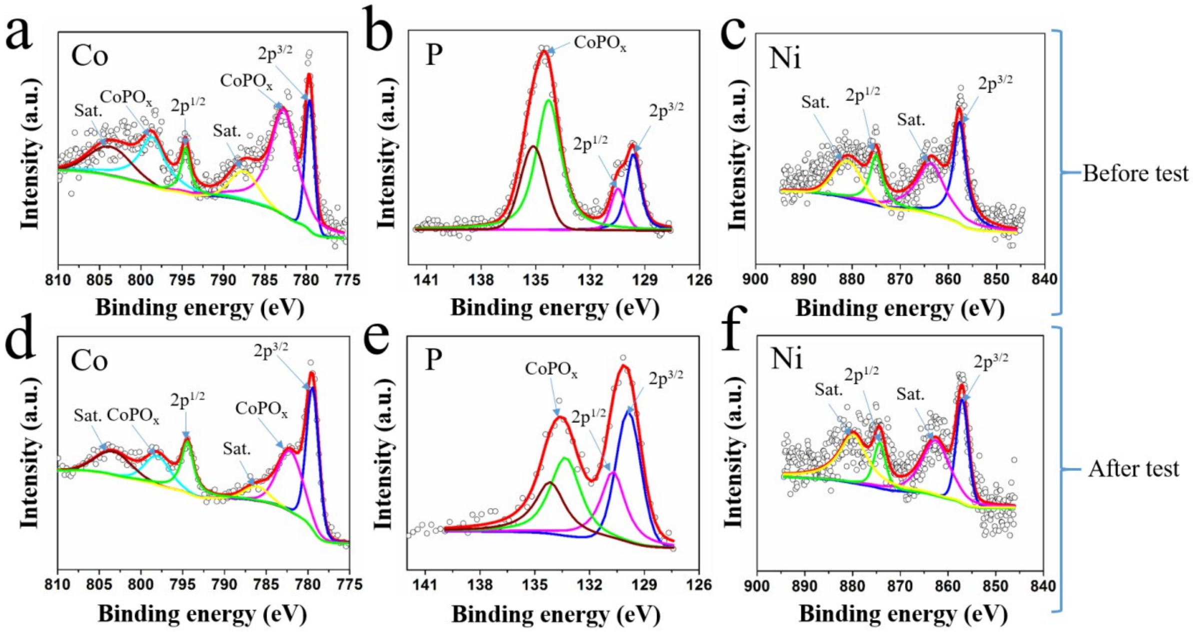

Figure S22. High resolution XPS spectra of as-prepared CoP/Ni_5P_4/CoP sample. (a-c) Before electrochemical test. (d-f) After electrochemical test in 0.5 M H_2SO_4.

Table S5. Comparison of the catalytic HER performance among our as-obtained catalyst andh other available metal phosphide catalysts in the literatures. Here, $\eta_{10,}$ and η_{100} are denoted as the overpotentials at current density of 10, and 100 mA cm^{-2}, respectively. Electrolyte: 1 M KOH.

Catalysts	η_{10}	η_{100}	Tafel slope	Source
CoP/Ni_5P_4/CoP	71 mV	138 mV	58 mV dec^{-1}	This work
CoNiP	155 mV	NA	103 mV dec^{-1}	7
CoP nanowires	209 mV	537 mV	129 mV dec^{-1}	8
np-$(Co_{0.52}Fe_{0.48})_2P$	79 mV	176 mV	40 mV dec^{-1}	10
FeP nanorods	218 mV	NA	146 mV dec^{-1}	17
Ce-doped CoP	92 mV	161 mV	63.5 mV dec^{-1}	14
CoMoP	81 mV	NA	55.5 mV dec^{-1}	21
Co_2P nanorods	152 mV	NA	NA	13

NA: Not applicable since not reported. The symbol "*" means that the value is extracted on the basis of the Tafel slope and overpotential at 10 mA cm^{-2}.

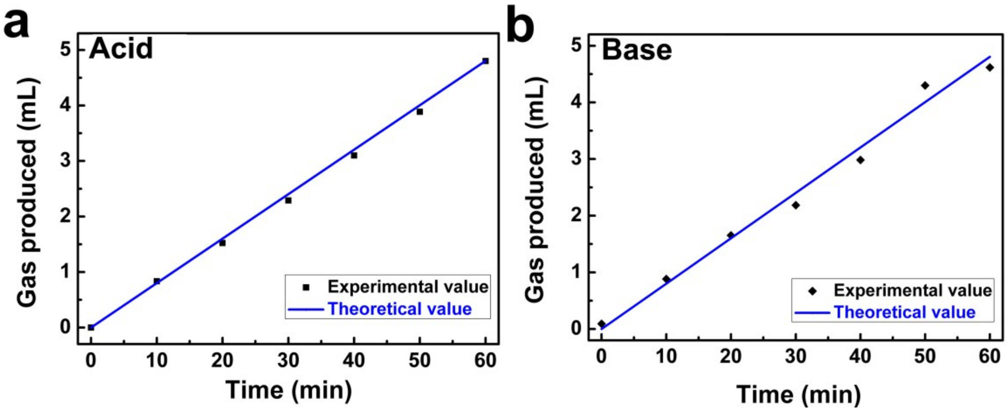

Figure S23. Measuring the gas products and determining the corresponding Faradaic efficiency using gas chromatography (GC) technique. The comparison between the experimental (black color) and theoretical (blue line) H_2 amounts in acid (a) and base (b) media. A volume of 0.3 mL gas sample was injected into the chromatography at different time of electrolysis in acid (a) and base (b). Current density: -50 mA cm^{-2}.

References

1. H. Q. Zhou, F. Yu, Y. Huang, J. Y. Sun, Z. Zhu, R. J. Nielsen, R. He, J. M. Bao, W. A. Goddard III, S. Chen, Z. F. Ren, *Nat. Commun.* **2016**, *7*, 12765.
2. D. Merki, S. Fierro, H. Vrubel, X. L. Hu, *Chem. Sci.* **2011**, *2*, 1262.
3. Y. Y. Chen, Y. Zhang, X. Zhang, T. Tang, H. Luo, S. Niu, Z. H. Dai, L. J. Wan, J. S. Hu. *Adv. Mater.* **2017**, *29*, 1703311.
4. C. Tang, L. Gan, R. Zhang, W. Lu, X. Jiang, A. M. Asiri, X. Sun, J. Wang, L. Chen, *Nano Lett.* **2016**, *16*, 6617.
5. M. C. Acevedo, M. L. Stone, J. R. Schmidt, J. G. Thomas, Q. Ding, H. C. Chang, M. L. Tsai, J. H. He and S. Jin, *Nat. Mater.* **2015**, 14, 1245.
6. I. K. Mishra, H. Q. Zhou, J. Y. Sun, K. Dahal, Z. S. Ren, R. He, S. Chen, Z. F. Ren, *Mater. Today Phys.* **2018**, *4*, 1.
7. A. Han, H. Chen, H. Zhang, Z. Sun, P. Du, *J. Mater. Chem. A* **2016**, *4*, 10195.
8. J. Tian, Q. Liu, A. M. Asiri, X. Sun, *J. Am. Chem. Soc.* **2014**, *136*, 7587.

9. X. L. Yang, A. Y. Lu, Y. H. Zhu, M. N. Hedhili, S. X. Min, K. W. Huang, Y. Han and L. J. Li, *Nano Energy* **2015**, *15*, 634.
10. Y. W. Tan, H. Wang, P. Liu, Y. H. Shen, C. Cheng, A. Hirata, T. Fujita, Z. Tang and M. W. Chen, *Energy Environ. Sci.* **2016**, *9*, 2257.
11. E. J. Popczun, C. G. Read, C. W. Roske, N. S. Lewis and R. E. Schaak, *Angew. Chem. Int. Ed.* **2014**, *53*, 5427.
12. Q. Liu, J. Q. Tian, W. Cui, P. Jiang, N. Y. Cheng, A. M. Asiri and X. P. Sun, *Angew. Chem. Int. Ed.* **2014**, *53*, 6710.
13. Z. P. Huang, Z. Z. Chen, Z. B. Chen, C. C. Lv, M. G. Humphrey, C. Zhang, *Nano Energy* **2014**, *9*, 373.
14. W. Gao, M. Yan, H. Y. Cheung, Z. M. Xia, X. M. Zhou, Y. B. Qin, C. Y. Wong, J. C. Ho, C. R. Chang, Y. Q. Qu, *Nano Energy* **2017**, *38*, 290.
15. E. J. Popczun, J. R. McKone, C. G. Read, A. J. Biacchi, A. M. Wiltrout, N. S. Lewis and R. E. Schaak, *J. Am. Chem. Soc.* **2013**, *135*, 9267.
16. Z. P. Huang, Z. B. Chen, Z. Z. Chen, C. C. Lv, H. Meng, C. Zhang, *ACS Nano* **2014**, *8*, 8121.
17. Y. H. Liang, Q. Liu, A. M. Asiri, X. P. Sun and Y. L. Luo, *ACS Catal.* **2014**, *4*, 4065.
18. P. Jiang, Q. Liu, Y. H. Liang, J. Q. Tian, A. M. Asiri, X. P. Sun, *Angew. Chem. Int. Ed.* **2014**, *53*, 12855.
19. J. Q. Tian, Q. Liu, N. Y. Cheng, A. M. Asiri, and X. P. Sun, *Angew. Chem. Int. Ed.* **2014**, *53*, 9577.
20. W. Liu, E. Hu, H. Jiang, Y. Xiang, Z. Weng, M. Li, Q. Fan, X. Yu, E. I. Altman, H. Wang*, Nat. Commun*. **2016**, *7*, 10771.
21. Y. Y. Ma, C. X. Wu, X. J. Feng, H. Q. Tan, L. K. Yan, Y. Liu, Z. H. Kang, E. B. Wang, Y. G. Li, *Energy Environ. Sci.* **2017**, *10*, 788.
22. X. D. Wang, Y. F. Xu, H. S. Rao, W. J. Xu, H. Y. Chen, W. X. Zhang, D. B. Kuang, C. Y. Su, *Energy Environ. Sci.* **2016**, *9*, 1468.
23. M. Pi, T. Wu, D. Zhang, S. Chen, S. Wang, *Nanoscale* **2016**, *8*, 19779.

24. P. Xiao, M. A. Sk, L. Thia, X. Ge, R. J. Lim, J. Y. Wang, K. H. Lima, X. Wang, *Energy Environ. Sci.* **2014**, *7*, 2624.
25. Z. C. Xing, Q. Liu, A. M. Asiri and X. P. Sun, *Adv. Mater.* **2014**, *26*, 5702.
26. J. Kibsgaard, T. F. Jaramillo, *Angew. Chem. Int. Ed.* **2014**, *53*, 14433.
27. H. Q. Zhou, F. Yu, J. Y. Sun, H. T. Zhu, I. K. Mishra, S. Chen, Z. F. Ren, *Nano Lett.* **2016**, *16*, 7604.
28. X. Long, V. Li, Z. Wang, H. Y. Zhu, T. Zhang, S. Xiao, W. Guo, S. Yang, *J. Am. Chem. Soc.* **2015**, *137*, 11900.
29. D. Kong, H. Wang, Z. Lu, Y. Cui, *J. Am. Chem. Soc.* **2014**, *136*, 4897.
30. H. Q. Zhou, F. Yu, Y. Y. Liu, J. Y. Sun, Z. Zhu, R. He, J. M. Bao, W. A. Goddard III, S. Chen, Z. F. Ren, *Energy Environ. Sci.* **2017**, *10*, 1487.
31. J. Kibsgaard, C. Tsai, K. Chan, J. D. Benck, J. K. Nørskov, F. Abild-Pedersen, T. F. Jaramillo, *Energy Environ. Sci.* **2015**, *8*, 3022.